Adsorption 9: 251–264, 2003

Simulation of a Combined Isomerization Reactor & Pressure Swing Adsorption Unit

ABDULHADI A. AL-JUHANI AND KEVIN F. LOUGHLIN*
Department of Chemical Engineering, King Fahd University of Petroleum & Minerals, Dhahran 31261, Saudi Arabia
aljuhani@kfupm.edu.sa
loughkf@kfupm.edu.sa

Abstract. The Total Isomerization Process developed by Union Carbide in 1970 (Gary, 1987) for the conversion of normal paraffin's to their isomers consists of a reactor followed by a PSA unit each operating at similar pressures and temperatures. The combination of these two operations in one unit in a Pressure Swing Adsorption Reactor (PSAR) process may provide an increased throughput and a significant cost saving in ancillary equipment.

The simulation of a mathematical model linking the catalyst packed-bed and the adsorbent packed-bed is reported. The catalyst is a Pd/Y-zeolite and the adsorbent is 5A zeolite. The simulated feed consists of 17% each of n- and isopentane with the remainder being hydrogen. The mathematical model assumes dispersed plug-flow in both sections, constant velocity in the reactor section but varying in the adsorber, with mass transfer in the adsorber section due to external fluid film resistance and macropore diffusion in series. The fraction of the total column length occupied by the catalyst (denoted by ω) is accounted for in the model by solving numerically using orthogonal collocation on finite elements. Parameters varied are the ratio of catalyst/column length (ω), temperature range (506–533 K), high pressure (15–20 bars), with the low pressure held constant at 2 bars. The catalyst/column ratio has a strong effect at low temperatures. The optimum catalyst/column length ratio appears to be controlled by the low pressure step and occurs at $\omega = 0.7$ for the assumptions used in this work.

Keywords: isomerization, pressure swing adsorption reactor, simulation, n-pentane, isopentane

Introduction

The isomerization of n-paraffins to high-octane number branched isomers for upgrading naphtha is of strong commercial interest. Light straight-run naphtha, consisting mainly of n-pentane and n-hexane, is partially isomerized via an isomerization reactor and the products are separated. The unreacted n-paraffins are recycled to the reactor. Separation by distillation is difficult and energy consuming because the n-/isoparaffins mixture is composed of components with close-boiling points. The separation can be performed by selective adsorption using molecular sieves such as 5A zeolite, where the n-paraffins are adsorbed and the iso-paraffins are excluded (Minkkinen et al., 1993; Morbidelli et al., 1996).

This method is widely used in industry, such as the Total Isomerization Process (TIP) developed by Union Carbide in 1970 (Gary, 1987). The block-flow diagram for the TIP process is shown in Fig. 1. In the diagram, the reactor typically operates most efficiently at high pressures (200–400 psia). The reaction must be conducted in the presence of hydrogen to avoid deactivation of the catalyst. Depending on the particular catalyst composition employed, the operating temperature of the isomerization reactor is generally within the range of 200 to 390°C. The minimum hydrogen partial pressure required is also dependent on the catalyst used,

*To whom correspondence should be addressed.

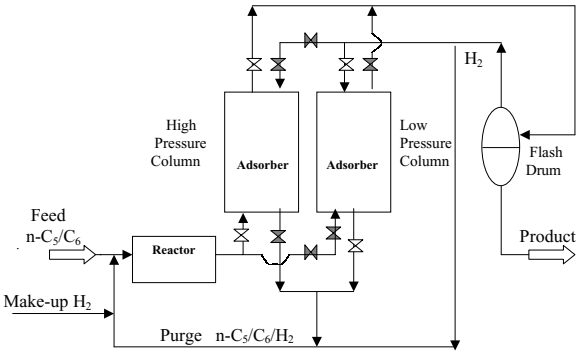

Figure 1. Block-flow diagram for the total isomerization process.

and is usually in the range of 100 to 250 psia. Adsorber units have typically operated more efficiently at lower pressures (200–300 psia). Typical properties of the TIP process, as in the patent published by Gary (1987), are summarized in Table 1.

The objective of this research work is to develop and simulate a model that describes a combined reactor/pressure swing adsorber unit (PSAR), for isomerizing n-pentane to its branched isomers. The concept of combining reaction and separation is not new as may be observed in membrane reactors, reactive distillation units, and others (Fogler, 1992). The pressure-swing reactor is a relatively new and untested device that combines reaction and product separation in a plant resembling a pressure swing adsorption (PSA) system (Alpay et al., 1993; Chatsiriwech et al., 1994; Goto et al., 1993; Kirkby and Morgan, 1994). In this device, a mixture of a catalyst and an adsorbent is filled in a chemical reactor. Mixing of the sorbent with the catalyst can be done in either a homogeneous or heterogeneous way (Lee and Kadlec, 1989). In homogeneous units, the catalyst and the adsorbent are mixed uniformly, and one of the reaction products should be the strongly adsorbed component in order to get higher conversion by shifting the conversion to the right. Heterogeneous units are formed by dividing the unit into two separate regions; the catalyst-packed bed region followed by the adsorbent-packed bed region. Here, the strongly adsorbed component can be either the reactant or the product.

Table 1. Typical properties of the Total Isomerization Process (Gary, 1987).

Fresh feedstock composition	
Components	Weight %
C_4 and lower	4.1
i-C_5	24.5
n-C_5	27.8
i-C_6	14.7
n-C_6	27.4
C_7 and higher	1.5
Reactor condition	
• Catalyst	0.1–1.0 wt % Pt (Pd)/Y-zeolite
• Pressure	14–28 bar
• Temperature	200–390°C
• H_2 partial pressure	7–14 bar
• H_2 feed composition	50–70 mol %
Adsorbers condition	
• Adsorbent	5A zeolite
• No. of beds	4
• No. of steps/bed	4 (basic Skarstrom cycle)
• Pressure at adsorption step	14–20 bar
• Temperature	200–390°C
• Cyclic duration	2 min/step; 8 min/cycle

An excellent literature review on PSR systems has been given by Sircar et al. (1996). Studies on homogeneous PSAR systems have been reported by Vaporciyan and Kadlec (1987, 1989, 1993), Lu and Rodrigues (1994), Alpay et al. (1993, 1995, 1998), and by Sircar et al. (1996). In these studies, the main objective of applying the homogeneous PSR concept is to increase the conversion to a value higher than the equilibrium value by shifting the equilibrium reaction to the right. For the current study, however, the heterogeneous PSAR concept will be applied because the main objective here is to reduce the required unit operation equipment.

Proposed Process

The block-flow diagram of the proposed PSAR system, taking the example of n-paraffins isomerization reaction, is shown in Fig. 2. In this figure, the heterogeneous mixing system is employed and the reactant is the strongly adsorbed component.

The catalyst selected for the hydroisomerization of n-C_5/i-C_5 mixtures was a 0.5 wt% Pd/H-faujasite which had been studied experimentally in 1982 by Bryant and Spivey (Bryant and Voorhies, 1968; Bryant and Spivey, 1982). The rate constant values for a temperature range of 506 to 533 K are given in the paper. Catalyst deactivation is assumed negligible when

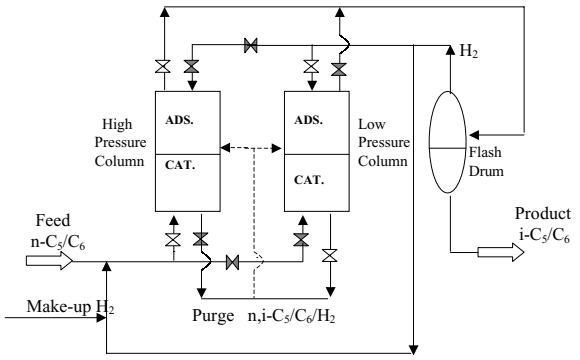

Figure 2. Flow diagram for the combined isomerization reactor/adsorber PSAR process.

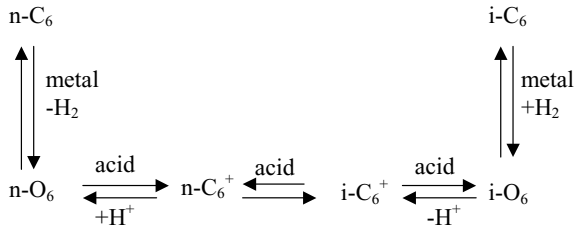

Figure 3. Weisz bifunctional mechanism. (n-C_6: n-hexane; n-O_6: n-hexene; n-C_6^+: n-carbonium ion; i-C_6^+: iso-carbonium ion; i-O_6: iso-hexene; i-C_6: iso-hexane.) (1962)

modeling which is reasonable for this system. The adsorbent used was 5A zeolite for which data have been reported by Silva and Rodrigues (1997a, 1997b) for this system.

The performance of a PSAR unit can be affected by a number of design parameters, such as the bed length and the adsorbent/catalyst size; operating parameters, such as the duration of the various steps and the pressure level in each step; and physical/chemical parameters, such as adsorption isotherm relationship and reaction rate constant. The effects of these parameters are coupled so that it is difficult to arrive at an optimal design only by experimentation. Therefore, reliable mathematical modeling and computer simulations are required to obtain preliminary information about the performance of the PSAR process in order to insure that the capital and/or operating costs are minimized while satisfying technical specifications such as conversion, yield, and product purity.

Theoretical Model

Assumptions

The dynamic model is based on the following assumptions:

1. The gas is assumed ideal (the temperature is high ∼500 K and the hydrogen content is high ∼50%).
2. The flow pattern is described by the axial dispersed plug flow model.
3. The gas and solids physical properties are independent of temperature. The model is assumed isothermal for this initial study.
4. The velocity is assumed constant in the reactor due to stoichiometry. The reaction is isothermal (Runstraat et al., 1997a, 1997b, 1997c).
5. The reaction rate is given by: $(-r_A) = k_1[c_A - \frac{c_B}{K_C}]$ (moles nC_5 consumed/hr/g. cat.) where subscripts A and B denote n-pentane and iso-pentane, respectively. This expression assumes an elementary first-order reversible reaction, with isomerization of the reactive intermediate to be the rate-controlling step. The reaction is shown in Fig. 3 as the Weisz Bifunctional Mechanism.
6. Deactivation of the catalyst is negligible. This is acceptable for a faujasite (Y zeolite) catalyst.
7. Hydrocracking products are negligible (Fajula et al., 1996).
8. The total pressure is constant during the sorption-desorption steps.
9. Mass transfer between fluid and solid phases are considered for all PSA steps. The main resistance to mass transfer in the adsorbent region are external fluid film resistance and macropore diffusion in series. These two resistances are combined in a global resistance Linear Driving Force (LDF) model according to a lumped model suggested by Morbidelli et al. (1982).
10. The effect of pressure is incorporated in the overall mass transfer coefficient (Ruthven et al., 1985; Ruthven and Raghavan, 1985).
11. The adsorption equilibrium is described by the Nitta et al. (1984) model as in Eq. (30).
12. A linear relationship is assumed for the pressure profile during the pressurization and the blowdown steps.
13. The frictional pressure drop through the catalyst and the adsorbent beds is neglected.
14. Variation in the fluid velocity along the adsorber length is considered.

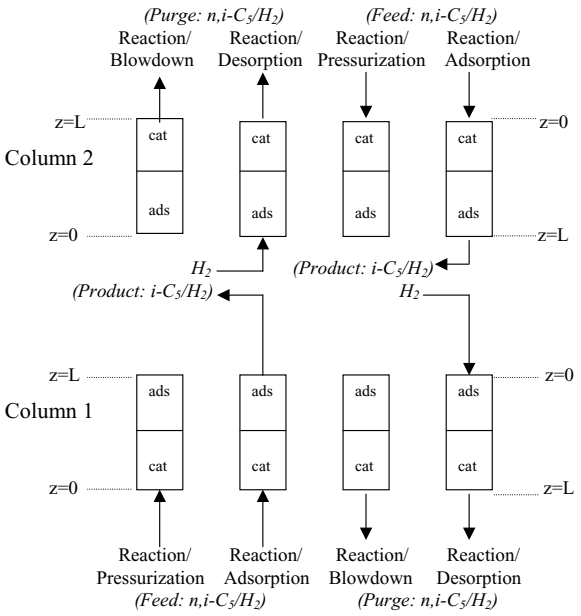

Figure 4. Proposed cyclic steps for the PSAR unit.

Figure 2 is the proposed process flow diagram for isomerizing of n-alkanes to isoalkanes in the PSAR unit. The unit consists of two columns. Each column consists of a catalyst-packed region followed by an adsorbent-packed region. For simplicity, the system is initially modeled as an isothermal process containing only three components (n-i/C_5/H_2). The cyclic steps of the PSAR scheme, shown in Fig. 4. are as follow:

Step 1: Pressurization/reaction. The unit is pressurized by feeding a portion of the feedstock (at high pressure) to it, injected into the catalyst bed. In the catalyst bed, partial conversion of n-C_5 to i-C_5 takes place. There is no effluent from the unit during this step.

Step 2: Reaction/adsorption. The feedstock (at high pressure) is fed to the catalyst bed where partial conversion of n-C_5 to i-C_5 takes place. Then, it enters the adsorbent region where unreacted n-C_5 is adsorbed. The effluent from the unit, composed of i-C_5 and hydrogen, is fed to a flash drum where i-C_5 is separated and taken off as the process product and H_2 is recycled to the process. This step continues until the adsorbent bed approaches a specified saturation limit. Then, feed is shut off, and step 3 is introduced.

Step 3: Blowdown/reaction. The unit is depressurized to a lower pressure level in a direction countercurrent to that of the feed gas flow. Desorption of n-C_5 takes place in the adsorbent region, followed by partial isomerization in the catalyst region. A gas stream containing all components of the system exits the unit. Usually this stream is considered as a waste stream and discharged off in most conventional PSA processes. In the present case, however, the blowdown stream should be utilized since it contains a considerable portion of i-C_5. The utilization of this gas stream will be studied in a future paper. In the present case, however, it will be considered as a waste stream to simplify the simulation.

Step 4: Desorption/reaction. Hydrogen gas, which is considered as inert, is introduced to the adsorbent bed at low pressure. This step desorbs the remaining n-C_5 from the adsorbent bed and forces it to the catalyst bed where partial isomerization takes places. Again the effluent in this step will be considered as a waste stream in the simulation.

Model Equations

A mathematical representation of the problem is as shown in Fig. 5. The normalized equations are written in terms of two-space variables, defined as follows:

$$\nu_1 = \frac{x}{\omega}; \quad 0 < x < \omega \tag{1a}$$

$$\nu_2 = \frac{x-\omega}{1-\omega}; \quad \omega < x < 1 \tag{1b}$$

In addition to the model assumptions listed above, the continuity of concentration, mass flux, and velocity at the junction of the two subdomains must be incorporated.

The normalized model equations are

Step 1 (Reaction/Pressurization)

$$\frac{\partial y_{A1}}{\partial \tau} = \frac{1}{\omega^2}\frac{1}{\mathrm{Pe}}\frac{\partial^2 y_{A1}}{\partial \nu_1^2} - \frac{1}{\omega}\frac{\partial (U_1 y_{A1})}{\partial \nu_1} - \frac{y_{A1}}{C_T}\frac{\partial C_T}{\partial \tau} - \frac{\mathrm{Da}_t}{\omega}\left[y_{A1} - \frac{y_{B1}}{K_C}\right] \tag{2}$$

$$\frac{\partial y_{B1}}{\partial \tau} = \frac{1}{\omega^2}\frac{1}{\mathrm{Pe}}\frac{\partial^2 y_{B1}}{\partial \nu_1^2} - \frac{1}{\omega}\frac{\partial (U_1 y_{B1})}{\partial \nu_1} - \frac{y_{B1}}{C_T}\frac{\partial C_T}{\partial \tau} + \frac{\mathrm{Da}_t}{\omega}\left[y_{A1} - \frac{y_{B1}}{K_C}\right] \tag{3}$$

$$\frac{\partial U_1}{\partial \nu_1} = -\frac{\omega}{C_T}\frac{\partial C_T}{\partial \tau} \tag{4}$$

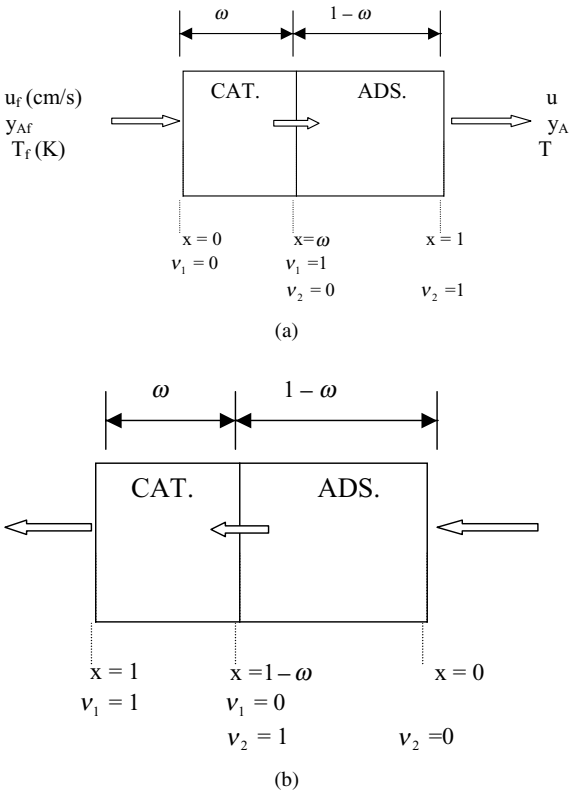

Figure 5. (a) Mathematical representation for the PSAR unit (Steps 1 and 2). Note that for step 1 the product end is closed. (b) Mathematical representation for the PSAR unit (Steps 3 and 4). Note that for Step 3 the feed inlet is closed.

$$\frac{\partial y_{A2}}{\partial \tau} = \frac{1}{(1-\omega)^2}\frac{1}{\mathrm{Pe}}\frac{\partial^2 y_{A2}}{\partial \nu_2^2} - \frac{1}{(1-\omega)}\frac{\partial (U_2 y_{A2})}{\partial \nu_2} - \frac{y_{A2}}{C_T}\frac{\partial C_T}{\partial \tau} - \frac{1}{C_T}\zeta_m \frac{\partial Q_A}{\partial \tau} \tag{5}$$

$$\frac{\partial y_{B2}}{\partial \tau} = \frac{1}{(1-\omega)^2}\frac{1}{\mathrm{Pe}}\frac{\partial^2 y_{B2}}{\partial \nu_2^2} - \frac{1}{(1-\omega)}\frac{\partial (U_2 y_{B2})}{\partial \nu_2} - \frac{y_{B2}}{C_T}\frac{\partial C_T}{\partial \tau} \tag{6}$$

$$\frac{\partial U_2}{\partial \nu_2} = -\frac{(1-\omega)}{C_T}\frac{\partial C_T}{\partial \tau} - \frac{(1-\omega)}{C_T}\zeta_m \frac{\partial Q_A}{\partial \tau} \tag{7}$$

The boundary conditions are

$$x = 1, \tau > 0 \quad -\frac{1}{\mathrm{Pe}}\frac{\partial y_{A1}}{\partial \nu_1} = U_1|_{\nu_1=0}\omega(y_{Af} - y_{A1}) \tag{8a}$$

$$\nu_1 = 1, (\nu_2 = 0), \tau > 0 \quad y_{A1} = y_{A2} \tag{8b}$$

$$\nu_1 = 1, (\nu_2 = 0), \tau > 0 \quad -(1-\omega)D_A\frac{\partial y_{A1}}{\partial \nu_1} = -\omega D_A \frac{\partial y_{A2}}{\partial \nu_2} \tag{8c}$$

$$\nu_1 = 1, (\nu_2 = 0), \tau > 0 \quad U_1 = U_2 \tag{8d}$$

$$\nu_2 = 1, \tau > 0 \quad \frac{\partial y_{A2}}{\partial \nu_2} = 0 \tag{8e}$$

$$\nu_2 = 1, \tau > 0 \quad U_2 = 0 \tag{8f}$$

Step 2 (Reaction/Adsorption)

$$\frac{\partial y_{A1}}{\partial \tau} = \frac{1}{\omega^2}\frac{1}{\mathrm{Pe}}\frac{\partial^2 y_{A1}}{\partial \nu_1^2} - \frac{1}{\omega}\frac{\partial y_{A1}}{\partial \nu_1} - \frac{\mathrm{Da}_t}{\omega}\left[y_{A1} - \frac{y_{B1}}{K_C}\right] \tag{9}$$

$$\frac{\partial y_{B1}}{\partial \tau} = \frac{1}{\omega^2}\frac{1}{\mathrm{Pe}}\frac{\partial^2 y_{B1}}{\partial \nu_1^2} - \frac{1}{\omega}\frac{\partial y_{B1}}{\partial \nu_1} + \frac{\mathrm{Da}_t}{\omega}\left[y_{A1} - \frac{y_{B1}}{K_C}\right] \tag{10}$$

$$\frac{\partial y_{A2}}{\partial \tau} = \frac{1}{(1-\omega)^2}\frac{1}{\mathrm{Pe}}\frac{\partial^2 y_{A2}}{\partial \nu_2^2} - \frac{1}{(1-\omega)}\frac{\partial (U_2 y_{A2})}{\partial \nu_2} - \zeta_m \frac{\partial Q_A}{\partial \tau} \tag{11}$$

$$\frac{\partial y_{B2}}{\partial \tau} = \frac{1}{(1-\omega)^2}\frac{1}{\mathrm{Pe}}\frac{\partial^2 y_{B2}}{\partial \nu_2^2} - \frac{1}{(1-\omega)}\frac{\partial (U_2 y_{B2})}{\partial \nu_2} \tag{12}$$

$$\frac{\partial U_2}{\partial \nu_2} = -(1-\omega)\zeta_m \frac{\partial Q_A}{\partial \tau} \tag{13}$$

The boundary conditions are

$$\nu_1 = 0, \tau > 0 \quad -\frac{1}{\mathrm{Pe}}\frac{\partial y_{A1}}{\partial \nu_1} = \omega(y_{Af} - y_{A1}) \tag{14a}$$

$$\nu_1 = 1, (\nu_2 = 0), \tau > 0 \quad y_{A1} = y_{A2} \tag{14b}$$

$$\nu_1 = 1, (\nu_2 = 0), \tau > 0 \quad -(1-\omega)D_A\frac{\partial y_{A1}}{\partial \nu_1} = -\omega D_A \frac{\partial y_{A2}}{\partial \nu_2} \tag{14c}$$

$$\nu_2 = 0, \tau > 0 \quad U_2 = 1 \tag{14d}$$

$$\nu_2 = 1, \tau > 0 \quad \frac{\partial y_{A2}}{\partial \nu_2} = 0 \tag{14e}$$

$$\nu_1 = 1, (\nu_2 = 0), \tau > 0 \quad U_1 = U_2 \tag{14f}$$

Step 3 (Reaction/Blowdown)

$$\frac{\partial y_{A1}}{\partial \tau} = \frac{1}{\omega^2}\frac{1}{\mathrm{Pe}}\frac{\partial^2 y_{A1}}{\partial \nu_1^2} - \frac{1}{\omega}\frac{\partial (U_1 y_{A1})}{\partial \nu_1} - \frac{y_{A1}}{C_T}\frac{\partial C_T}{\partial \tau} - \frac{\mathrm{Da}_t}{\omega}\left[y_{A1} - \frac{y_{B1}}{K_C}\right] \tag{15}$$

$$\frac{\partial y_{B1}}{\partial \tau} = \frac{1}{\omega^2}\frac{1}{\mathrm{Pe}}\frac{\partial^2 y_{B1}}{\partial \nu_1^2} - \frac{1}{\omega}\frac{\partial (U_1 y_{B1})}{\partial \nu_1} - \frac{y_{B1}}{C_T}\frac{\partial C_T}{\partial \tau} + \frac{\mathrm{Da}_t}{\omega}\left[y_{A1} - \frac{y_{B1}}{K_C}\right] \tag{16}$$

$$\frac{\partial U_1}{\partial \nu_1} = -\frac{\omega}{C_T}\frac{\partial C_T}{\partial \tau} \tag{17}$$

$$\frac{\partial y_{A2}}{\partial \tau} = \frac{1}{(1-\omega)^2}\frac{1}{\mathrm{Pe}}\frac{\partial^2 y_{A2}}{\partial \nu_2^2} - \frac{1}{(1-\omega)}\frac{\partial (U_2 y_{A2})}{\partial \nu_2} - \frac{y_{A2}}{C_T}\frac{\partial C_T}{\partial \tau} - \frac{1}{C_T}\zeta_m\frac{\partial Q_A}{\partial \tau} \tag{18}$$

$$\frac{\partial y_{B2}}{\partial \tau} = \frac{1}{(1-\omega)^2}\frac{1}{\mathrm{Pe}}\frac{\partial^2 y_{B2}}{\partial \nu_2^2} - \frac{1}{(1-\omega)}\frac{\partial (U_2 y_{B2})}{\partial \nu_2} - \frac{y_{B2}}{C_T}\frac{\partial C_T}{\partial \tau} \tag{19}$$

$$\frac{\partial U_2}{\partial \nu_2} = -\frac{(1-\omega)}{C_T}\frac{\partial C_T}{\partial \tau} - \frac{(1-\omega)}{C_T}\zeta_m\frac{\partial Q_A}{\partial \tau} \tag{20}$$

The boundary conditions are

$$\nu_2 = 0, \tau > 0 \quad \frac{\partial y_{A2}}{\partial \nu_2} = 0 \tag{21a}$$

$$\nu_1 = 0, (\nu_2 = 1), \tau > 0 \quad y_{A1} = y_{A2} \tag{21b}$$

$$\nu_1 = 0, (\nu_2 = 1), \tau > 0$$
$$-(1-\omega)D_A\frac{\partial y_{A1}}{\partial \nu_1} = -\omega D_A\frac{\partial y_{A2}}{\partial \nu_2} \tag{21c}$$

$$\nu_1 = 0, (\nu_2 = 1), \tau > 0 \quad U_1 = U_2 \tag{21d}$$

$$\nu_1 = 1, \tau > 0 \quad \frac{\partial y_{A1}}{\partial \nu_1} = 0 \tag{21e}$$

$$\nu_2 = 0, \tau > 0 \quad U_2 = 0 \tag{21f}$$

Step 4 (Reaction/Desorption)

$$\frac{\partial y_{A1}}{\partial \tau} = \frac{1}{\omega^2}\frac{1}{\mathrm{Pe}}\frac{\partial^2 y_{A1}}{\partial \nu_1^2} - \frac{1}{\omega}\frac{\partial (U_1 y_{A1})}{\partial \nu_1} - \frac{\mathrm{Da}_t}{\omega}\left[y_{A1} - \frac{y_{B1}}{K_C}\right] \tag{22}$$

$$\frac{\partial y_{B1}}{\partial \tau} = \frac{1}{\omega^2}\frac{1}{\mathrm{Pe}}\frac{\partial^2 y_{B1}}{\partial \nu_1^2} - \frac{1}{\omega}\frac{\partial (U_1 y_{B1})}{\partial \nu_1} + \frac{\mathrm{Da}_t}{\omega}\left[y_{A1} - \frac{y_{B1}}{K_C}\right] \tag{23}$$

$$\frac{\partial U_1}{\partial \nu_1} = 0 \tag{24}$$

$$\frac{\partial y_{A2}}{\partial \tau} = \frac{1}{(1-\omega)^2}\frac{1}{\mathrm{Pe}}\frac{\partial^2 y_{A2}}{\partial \nu_2^2} - \frac{1}{(1-\omega)}\frac{\partial (U_2 y_{A2})}{\partial \nu_2} - \frac{1}{C_T}\zeta_m\frac{\partial Q_A}{\partial \tau} \tag{25}$$

$$\frac{\partial y_{B2}}{\partial \tau} = \frac{1}{(1-\omega)^2}\frac{1}{\mathrm{Pe}}\frac{\partial^2 y_{B2}}{\partial \nu_2^2} - \frac{1}{(1-\omega)}\frac{\partial (U_2 y_{B2})}{\partial \nu_2} \tag{26}$$

$$\frac{\partial U_2}{\partial \nu_2} = -\frac{(1-\omega)}{C_T}\zeta_m\frac{\partial Q_A}{\partial \tau} \tag{27}$$

The boundary conditions are

$$\nu_2 = 0, \tau > 0 \quad \frac{1}{\mathrm{Pe}}\frac{\partial y_{A2}}{\partial \nu_2} = U_2|_{\nu_2=0}(1-\omega)y_{A2} \tag{28a}$$

$$\nu_1 = 0, (\nu_2 = 1), \tau > 0 \quad y_{A1} = y_{A2} \tag{28b}$$

$$\nu_1 = 0, (\nu_2 = 1), \tau > 0$$
$$-(1-\omega)D_A\frac{\partial y_{A1}}{\partial \nu_1} = -\omega D_A\frac{\partial y_{A2}}{\partial \nu_2} \tag{28c}$$

$$\nu_1 = 0, (\nu_2 = 1), \tau > 0 \quad U_1 = U_2 \tag{28d}$$

$$\nu_1 = 1, \tau > 0 \quad \frac{\partial y_{A1}}{\partial \nu_1} = 0 \tag{28e}$$

$$\nu_2 = 0, \tau > 0 \quad U_2 = u_p/u_f \tag{28f}$$

In all the four steps, the mass transfer rate and the adsorption equilibrium isotherm for the adsorbent region are

$$\zeta_m\frac{\partial Q_A}{\partial \tau} = N_f C_T(y_{A2} - \langle y_{A2}\rangle) \tag{29}$$

$$\langle y_{A2}\rangle P = \frac{1}{K_{ads}}\frac{\theta_{ref}Q_A}{(1-\theta_{ref}Q_A)^n} \tag{30}$$

The initial conditions are

$$y_{A1} = y_{B1} = y_{A2} = y_{B2} = Q_A = 0 \tag{31a}$$

$$y_{B1}(\nu_1, \tau = 0) = 0 \tag{31b}$$

$$y_{A2}(\nu_2, \tau = 0) = 0 \tag{31c}$$

$$y_{B2}(\nu_2, \tau = 0) = 0 \tag{31d}$$

$$Q_A(\nu_2, \tau = 0) = 0 \tag{31e}$$

In the above dimensionless equations, model parameters are defined as follows:

Damköhler number: $\mathrm{Da}_t = \dfrac{k_1\omega L}{u_f}$

Mass Peclet number: $\mathrm{Pe} = \dfrac{u_f L}{D_L}$

Mass capacity factor: $\zeta_m = \dfrac{1-\varepsilon}{\varepsilon}\dfrac{\rho_s q_{A,ref}}{c_{Tf}}$

Number of film mass-transfer units: $$N_f = \frac{1-\varepsilon}{\varepsilon}\frac{a_p k_{gl} L}{u_f}$$

Nonlinearity parameter of isotherm: $$\theta_{ref} = \frac{q_{A,ref}}{q_{max}}$$

Modeling Results

Model parameters were estimated from independent experiments and correlations available in the literature. Table 2 summarizes the column characteristics, adsorbent properties, and adsorption equilibrium isotherm and reaction parameters. The axial mass dispersion coefficient (D_L) is calculated approximately by:

$$D_L = 0.7D_m + 0.5ud_p \tag{32}$$

At low Reynolds number the second term in the above equation may be neglected (Runstraat et al., 1997c; Ruthven et al., 1985). The reaction equilibrium constants (K_C) were estimated from the correlation obtained by Pines and co-workers (Pines et al., 1945):

$$R \ln K_C = (1861/T) - 1.299 \tag{33}$$

Table 2. Data for the base-case system.

System: n-C_5/ i-C_5/H_2
Reactor and adsorption column characteristics
$L = 20$ cm and $2R_C = 3.35$ cm
Adsorbent properties
• $\rho_b = 0.77$ g/cm^3
• $\rho_s = 1.13$ g/cm^3
• $\varepsilon = 0.32$
• $\varepsilon_p = 0.35$
• $d_p = 1.6$ mm
• $a_p = 25$ cm^{-1}
Adsorption equilibrium isotherm parameters
• $-\Delta H_{ads} = 13.2$ kcal/mol
• $n = 5$
• $q_{max} = 13.0$ g/100 g
• $K_O = 2.013 * 10^{-5}$ bar $^{-1}$
Chemical reaction parameters
• $k_1 = 0.034$ s^{-1} @ 506 K
• $k_1 = 0.090$ s^{-1} @ 533 K

The overall mass transfer coefficient (k_{gl}) is calculated by using the lumped model proposed by Glueckauf (1955):

$$\frac{1}{k_{gl}} = \frac{1}{k_e} + \frac{1}{\varepsilon_p k_i} \tag{34}$$

where the intraparticle mass transfer coefficient (k_i) is calculated by:

$$k_i = \frac{5D_p}{R_p} \tag{35}$$

The external mass transfer coefficients (k_e) are estimated from the correlation obtained by Wakao and Kaguei (1982):

$$Sh = 2.0 + 1.1(Re)^{0.6}(Sc)^{0.33} \tag{36}$$

A qualitative analysis of the reaction unit operating at steady state was performed first by considering three basic parameters: the Peclet number, the Damköhler number, and the temperature. Parametric values used for simulation of the reaction unit are summarized in Table 3.

Figure 6 indicates the effect of dispersion on the concentration profile in the reactor. A low Peclet number indicates high dispersion, which lowers conversion. However, the effect is not very significant. Figure 7 indicates the effect of the kinetic parameter (the Damköhler number). Conversion increases with increasing Damköhler number until the equilibrium value is approached. Further increase of the

Table 3. Parametric values used for simulation of the reaction unit.

Parameter	Figure 6*	Figure 7*	Figure 8*
Varying parameter	Pe	Da	T
y_{Af}	0.17	0.17	0.17
y_{Bf}	0.17	0.17	0.17
T (K)	500	500	400, 500, 600
$y_{A,eq}$	0.077	0.077	0.053, 0.077, 0.097
K_C (–)	3.38	3.38	5.41, 3.38, 2.48
Pe (–)	20, 40, 100, 500	100	100
Da (–)	1.0	0.5, 1, 3, 10	1.0

**Note*: If a parameter in any column has more than one value, the first value corresponds to the first number of the varying parameter.

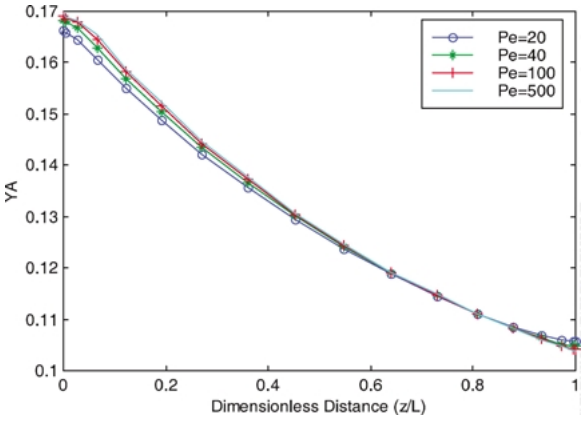

Figure 6. Concentration profile in the reactor (effect of dispersion). Parametric values are in Table 3.

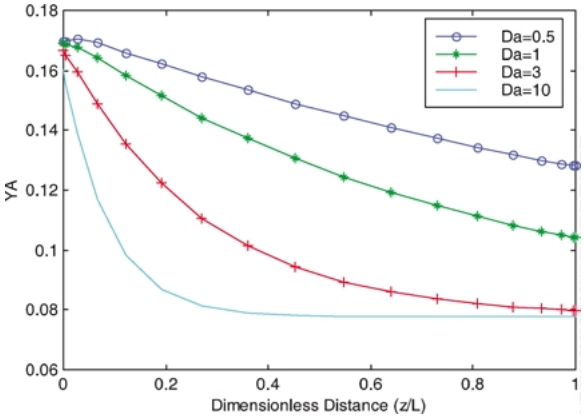

Figure 7. Concentration profile in the reactor (effect of Da number). Parametric values are in Table 3.

Damköhler number does not affect the outlet concentration. To reach the desired conversion near the equilibrium value, a minimum Damköhler number of approximately 3 is required as may be observed from Fig. 7. The Damköhler number can be increased by increasing the reactor length or by decreasing the feed flow rate. Therefore, an optimum value for the feed velocity is needed to get the desired values for the Peclet and the Damköhler numbers.

The effect of reaction temperature is shown in Fig. 8. In this isothermal model the heat of adsorption and desorption of nC_5/iC_5 is neglected but will be included in a nonisothermal model. Conversion is favorable at low temperatures. This is expected since the reaction is exothermic, whereas the reaction equilibrium constant is inversely proportional to temperature. The

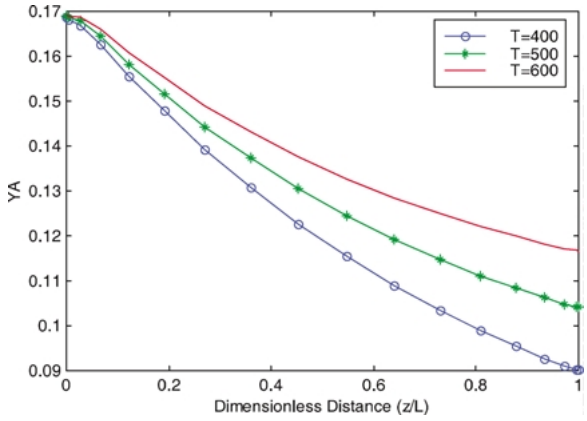

Figure 8. Concentration profile in the reactor (effect of temperature at Da = 1). Parametric values are in Table 3.

equilibrium values presented in Table 3 are calculated from the relationship $(y_{Af}+y_{Bf})/(K_C+1)$, which is derived from reaction stoichiometry. From the relation, it is clear that for a fixed feed concentration the equilibrium conversion increases as the temperature decreases. It is noticed in Fig. 8 that none of the three temperature runs reaches its equilibrium value. This is because the three runs are at low Damköhler number of 1. When the Damköhler number is increased to 5, all the three temperature runs reach their equilibrium values, as shown in Fig. 9.

A quantitative simulation analysis of a single PSAR column, which undergoes only step 2 (reaction/adsorption at constant high pressure) is considered. The objective is to review the breakthrough curves for the n-C_5/adsorbent system under the new column

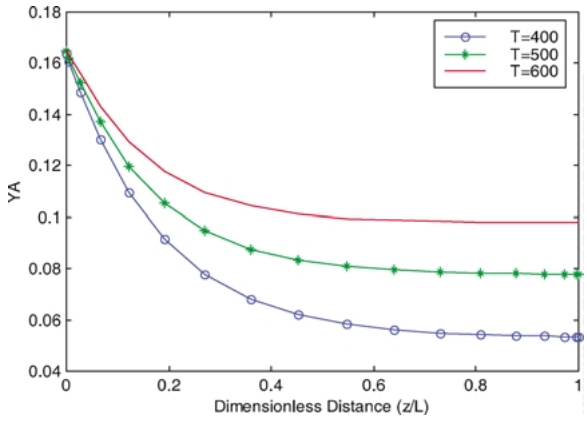

Figure 9. Concentration profile in the reactor (effect of temperature at Da = 5). Other parametric values are the same as for Fig. 7.

Table 4. Parametric values used for the solution of the breakthrough curves of the n-C_5/PSAR system.

Parameter	Figures 10 and 11*	Figure 12*	Figure 13*
Varying parameter	–	ω	ω
$y_{Af} = y_{Bf}$	0.17	0.17	0.17
F_f (mol/m^2/s)	0.15	0.15	0.15
P (bar)	15	15	15
T (K)	506	506	533
u_f (cm/s)	0.131	0.131	0.138
D_L (cm^2/s)	0.074	0.074	0.081
k_{gl} (cm/s)	0.62	0.62	0.67
K_{ads} (1/bar)	10.13	10.13	5.21
k_1 (1/s)	0.034	0.034	0.09
K_C (–)	3.31	3.31	3.01
$y_{A,eq}$ / y_{Af}	0.464	0.464	0.499
Pe	35.5	35.5	34.2
ζ_m	6.54	6.54	6.19
θ_{ref}	0.539	0.539	0.484
N_f	5039	5039	5150
Da_t	2.59	1.55, 2.59, 3.63	3.91, 9.13
ω	0.5	0.3, 0.5, 0.7	0.3, 0.7

**Note*: If a parameter in any column has more than one value, the first value corresponds to the first number of the varying parameter.

configuration at different operating conditions. Such a review will help in designing the cyclic PSAR process. Model parameters used in the simulation are presented in Table 4.

Figures 10 and 11 indicate the concentration profiles in the column for n-C_5 and i-C_5 respectively. The simulation is done at 506 K with ω equal to 0.5. The total time for this run is about 200 min. Figures 10 and 11 indicate that the concentration profiles in the catalyst region are time-independent after 20 min. In the adsorbent region, however, the concentration profiles change with time until reaching the breakthrough point, where the adsorbent bed is totally saturated with n-C_5. After that, the concentration profiles are uniform and equal to the exit concentrations from the catalyst bed. It should be noted that the concentration of i-C_5 reaches 28.3% in the adsorber section in the combined system whereas the highest value attained in the reactor on its own is only 26%. This is one of the benefits of using a PSAR reactor for this reaction.

Figures 12 and 13 indicate the effect of the ratio of catalyst to adsorbent in the column at 506 and 533 K,

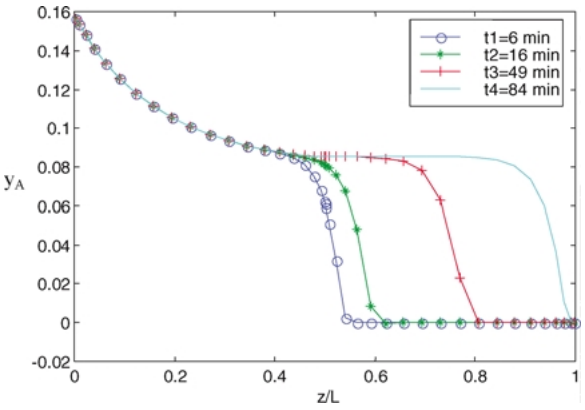

Figure 10. Concentration profiles in the fixed-bed PSAR column for n-C_5 in the gas phase. Parametric values are in Table 4.

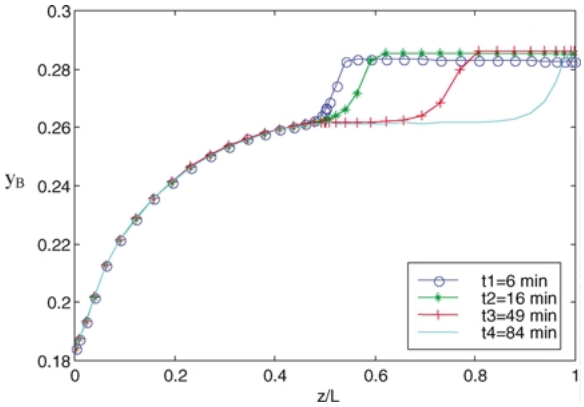

Figure 11. Concentration profiles in the fixed-bed PSAR column for i-C_5 in the gas phase. Parametric values are in Table 4.

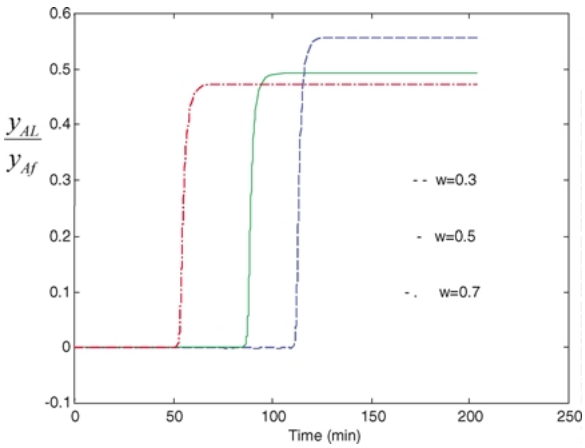

Figure 12. Breakthrough curve of the n,i-C_5/H_2/PSAR system (effect of catalyst/column length ratio at 506 K). Parametric values are in Table 4.

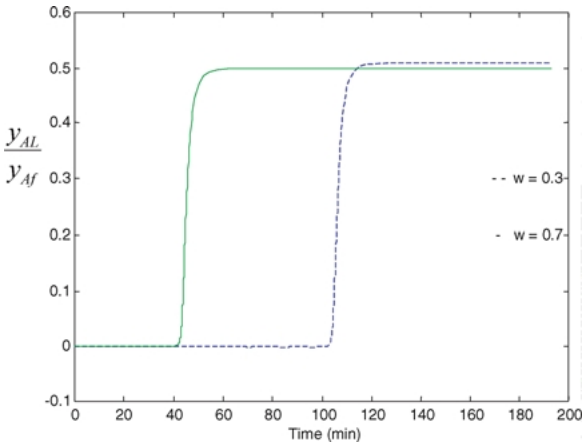

Figure 13. Breakthrough curve of the n,i-C_5/H_2/PSAR system (effect of catalyst/column length ratio at 533 K). Parametric values are in Table 4.

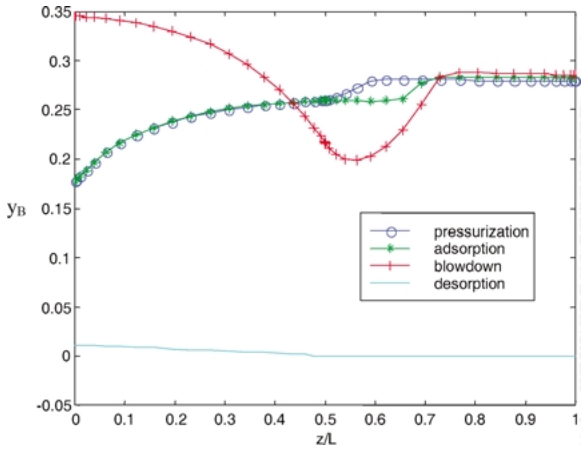

Figure 15. Gas phase concentration profiles of i-C_5 in the PSAR bed at the end of cyclic steady state ($\omega = 0.5$). Parametric values are the same as for Fig. 13.

respectively. The effect is dramatic at the lower temperature, where we need at least 70% of the column to be packed with the catalyst in order to get close to the equilibrium value. At the higher temperature, however, the effect is not so noticeable, where 50% catalyst packing is enough to get close to the equilibrium value. This different behavior is due to the large difference in the reaction rate constants at the two temperature (0.034 and 0.09 s^{-1} at 506 and 533 K, respectively), which results in a substantial difference in Damköhler numbers.

With the basic information obtained from modeling of the breakthrough curves for the fixed-bed PSAR column, the simulation of the four-steps PSAR cycle is now considered. The cycle starts initially with clean adsorbent and clean gas phase. The total length of the column is 20 cm. Parametric values used for simulations of the PSAR cycle are summarized in Table 5.

Figures 14 and 15 indicate the concentration profiles of n-C_5 and i-C_5 in the gas phase at the end of the four basic steps at cyclic steady state, respectively. The simulation is done at 506 K with ω equal to 0.5. The simulation is done also at the same conditions of Fig. 14, but with ω equal to 0.3 and 0.1, and the results are shown in Figs. 16 and 17.

Several conclusions can be drawn up from the above figures. At pressurization and adsorption steps, the

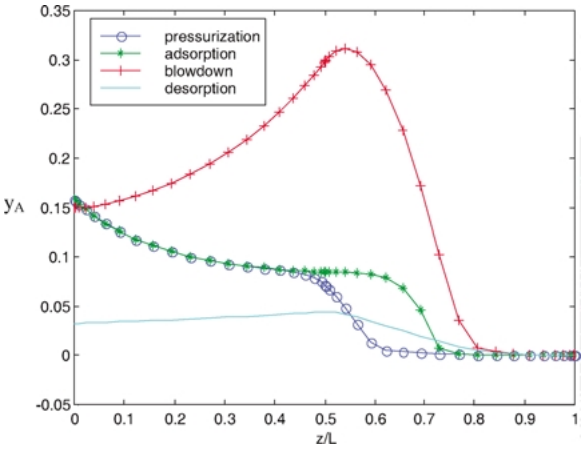

Figure 14. Gas phase concentration profiles of n-C_5 in the PSAR bed at the end of cyclic steady state ($\omega = 0.5$). Parametric values are in Table 5.

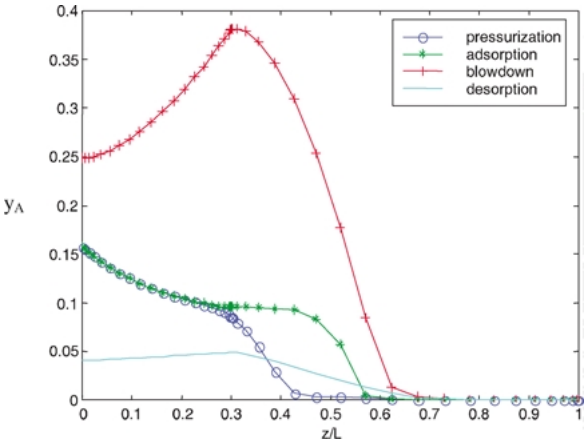

Figure 16. Gas phase concentration profiles of n-C_5 in the PSAR bed at the end of cyclic steady state ($\omega = 0.3$). Parametric values are in Table 5.

Table 5. Parametric values used for simulations of the n-C_5/PSAR system.

Parameter	Figures 14 and 15	Figure 16	Figure 17	Figure 18
$y_{Af} = y_{Bf}$	0.17	0.17	0.17	0.17
F_f (mol/m^2/s)	0.15	0.15	0.15	0.15
P_H (bar)	15	15	15	15
P_L (bar)	2	2	2	2
T (K)	506	506	506	533
u_f (cm/s)	0.131	0.131	0.131	0.138
Purge/ Feed volumetric ratio	3.0	3.0	3.0	3.0
D_L @ high pressure (cm^2/s)	0.074	0.074	0.074	0.081
D_L @ low pressure (cm^2/s)	0.555	0.555	0.555	0.608
k_{gl} @ high pressure (cm/s)	0.62	0.62	0.62	0.67
k_{gl} @ low pressure (cm/s)	2.23	2.23	2.23	2.31
k_1 (1/s)	0.034	0.034	0.034	0.09
K_C	3.31	3.31	3.31	3.01
K_{ads} (1/bar)	10.13	10.13	10.13	5.21
Pe @ high pressure	35.5	35.5	35.5	34.2
Pe @ low pressure	4.7	4.7	4.7	4.3
Pressurization & blowdown time (min)	7.69	7.69	7.69	7.25
Adsorption & desorption time (min)	15.38	15.38	15.38	14.5
$y_{A,eq}$	0.079	0.079	0.079	0.084
Da_t	2.59	1.55	0.518	varying
ω	0.5	0.3	0.1	varying
ζ_m	6.54	6.54	6.54	6.19
θ_{ref}	0.539	0.539	0.539	0.484

concentration decreases with position in the catalyst region due to reaction. The concentration of n-pentane at reaction equilibrium state (given by: $y_{A,eq} = (y_{Af} + y_{Bf})/(K_C+1)$) is equal to 0.079 at the given temperature

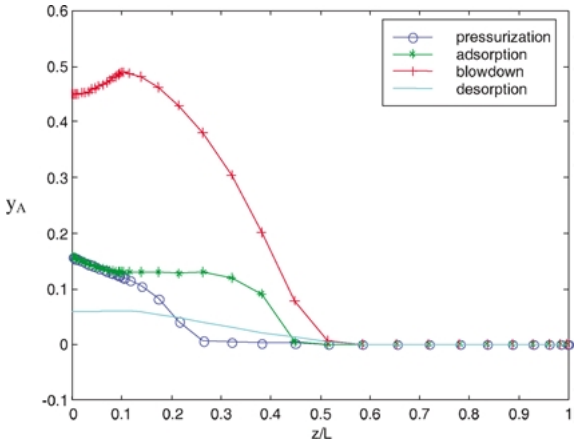

Figure 17. Gas phase concentration profiles of n-C_5 in the PSAR bed at the end of cyclic steady state ($\omega = 0.1$). Parametric values are in Table 5.

and feed concentrations. How close the concentration of n-pentane at the exit of the catalyst bed approaches to this equilibrium value depends on the catalyst/column length ratio, keeping the other operating conditions unchanged. As indicated in Figs. 14 and 16, the catalyst exit concentrations are 0.08 and 0.09 for ω values of 0.5 and 0.3, respectively. These results are close to the equilibrium value of 0.079. For ω equal to 0.1, however, the catalyst exit concentration is 0.12, as shown in Fig. 16. This is far above the equilibrium value, indicating that the catalyst bed length is not sufficient for the reaction.

At blowdown step, increasing concentration of n-pentane is due to desorption, and the rate of increase is higher at a lower value of ω. This is expected since a lower value of ω means higher adsorbent capacity. When n-pentane exits from the adsorbent region and enters the catalyst region, the concentration decreases with distance due to reaction. Here, the rate of decrease is highest at higher value of ω due to larger Damköhler number. The above observation is emphasized more clearly in Fig. 18, where the ratio of (y_B/y_A) in the column effluent at end of blowdown step is plotted

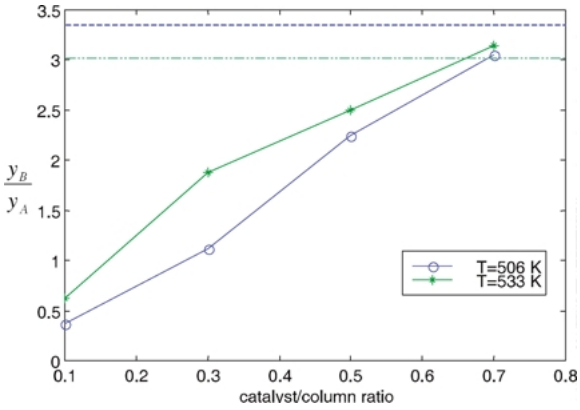

Figure 18. Effect of catalyst/adsorbent ratio on the exit concentration of n,i-C_5 in the gas phase at the end of blowdown step at cyclic steady state. Parametric values are in Table 5. (– – – – – – – – – – –, y_{BE}/y_{AE} @ 506 K, –··–··–··–··–··–··– , y_{BE}/y_{AE} @ 533 K).

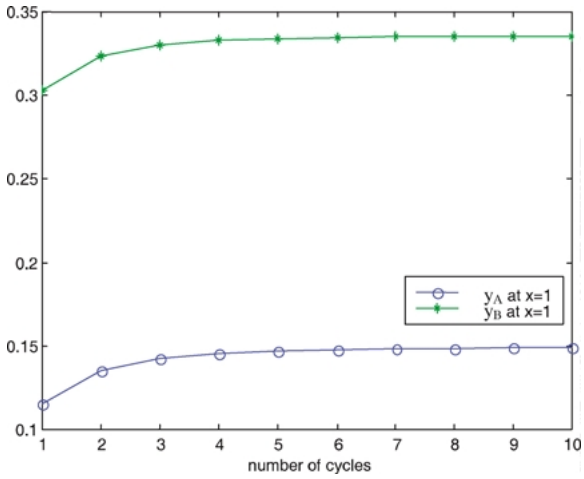

Figure 19. Approach to cyclic steady state, showing exit concentration of n-C_5 and i-C_5 at end of blowdown step. Parametric values are the same as that for Fig. 13.

against ω. The (product/reactant) concentration ratio increases as ω increases, and the relationship is almost linear. Results for another temperature of 533 K are also shown. The two temperatures have the same trend, with 533 K slightly better than 506 K for ω below 0.5, and almost the same performance for ω above 0.6. The equilibrium ratio y_{BE}/y_{AE} is 3.3 and 3.05 at 506 K and 533 K respectively and these values are shown on the diagram. This ratio is approached when $\omega = 0.7$ indicating the optimum ω is approximately 0.7 for the assumptions used in this study.

These results indicate that the blowdown effluent is valuable at moderate to higher catalyst/column length ratio, and should be utilized rather than discharged. One way to utilize the blowdown effluent is to feed it directly to the adsorbent region of the second column. This alternative is represented as the dash line in the block-flow diagram of the PSAR system (Fig. 2). This alternative suggests that there is perhaps a need to increase the diameter of the adsorbent region in order to take into account the increase in flow rate capacity.

As shown in Fig. 19, 10 cycles are needed in the simulations in order to reach cyclic steady state conditions. The number of cycles here is not high because the system is isothermal and contains one adsorbable component.

Another interesting conclusion can be observed from Fig. 17. At ω equals to 0.1, the concentration profiles of the PSAR system are similar to that of the PSA system which was also modeled (not shown). Thus, as ω approaches zero the PSAR model reduces to the PSA model. This indicates that the equations and computer simulation code developed are general in the sense that they can be used to solve the PSAR model as will as the base-case PSA model.

Conclusions

In the present study, theoretical investigation of n-C_5 isomerization reaction via the PSAR process has been carried out. The unit is packed with two separate layers of a Pd/Y-zeolite catalyst and a 5A zeolite adsorbent. A flowsheet diagram for the isomerization PSAR process is proposed, which consists of two columns with its associated valves and piping system. A cyclic scheme is proposed, which consists of four steps similar to the basic Skarstrom cycle (1960).

A mathematical model describing the dynamics of the PSAR process is developed. The model developed in the present study is general as it takes into account factors such as axial dispersion, resistance to mass transfer in the bulk phase, variable velocity along the column length, and mass exchange between bulk and solid phases during pressurization and blowdown steps.

The PSAR model developed is also used to simulate a four-step PSAR cyclic process. Parametric values used in the simulation are either obtained from experimental data or calculated from empirical correlations available in the literature without any adjustable parameters. The PSAR cycle is simulated at 506 and 533 K, and the catalyst/column length ratio is varied from 0.1 to 0.7. High-pressure feed step is at 15 bar, and low-pressure purge

step is at 2 bar. The catalyst/column length ratio should be at least 0.7 at both temperatures in order to get close to the equilibrium conversions in the desorption step.

Recommendations

Due to the significant changes in pressure from 2 to 20 bar in the process unit, a capacitance term should be included in the reactor section. Incorporation of recycle of the blowdown should be added to the model and the optimum position of this return feed location established.

The process needs to be simulated for nonisothermal operation and for operation with a mixture feed such as $nC_5/nC_6/iC_5/iC_6$.

Substitution of a membrane wall to both or either of the reactor or adsorber sections in lieu of solid walls should be developed. Placing the catalyst and/or adsorbent in a tubular membrane which only allows passage of H_2 will result in an enriched product stream being produced, and will also allow recovery of pure H_2 for the purging step. If the membrane-PSAR system is totally enclosed as in Fig. 20, self regulation is possible and additional purging may not be necessary. In self regulation, the H_2 diffuses out through the walls of the high pressure section and in through the walls of the low pressure section after having traversed the intervening medium thus providing an automatic self regulating purge. This flow reverses when the columns change pressure. This is a step our group is planning to examine.

Finally, the construction and testing of an experimental unit for comparison with predictions should be undertaken.

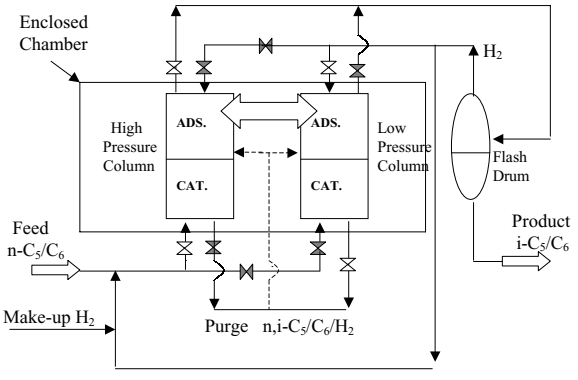

Figure 20. Hypothetical flowsheet for an enclosed membrane. Self regulating PSAR system.

Nomenclature

C_T	Dimensionless total gas concentration (mol/cm^3)
Da_t	True Damköhler number (–) $= \omega \frac{k_1 L}{u_f}$
D_L	Axial mass dispersion coefficient (cm^2/s)
D_A	Pore diffusivity of component A (cm^2/s)
k_1	Forward reaction rate constant (cm^3/g of cat/s)
K_{ads}	Adsorption equilibrium constant (bar^{-1})
k_{gl}	Global mass-transfer coefficient (cm/s)
K_C	Equilibrium reaction rate constant (–)
L	Length of the PSAR column (cm)
n	Coefficient of Nitta et al. isotherm (–)
N_f	Number of film mass-transfer units (–)
Pe	Mass Peclet number (–)
P	Total pressure (bar)
P_H	Constant high pressure during adsorption step (bar)
P_L	Constant low pressure during desorption step (bar)
Q_A	Dimensionless adsorbed-phase concentration (–)
Re	Particle Reynolds number
Sc	Schmidt number
T	Gas temperature (K)
u	Interstitial velocity (cm/s)
u_f	Interstitial feed velocity (cm/s)
U_i	Dimensionless interstitial velocity in bed i (–)
u_p	Purge gas velocity (cm/s)
x	Dimensionless axial coordinate in the column (–)
y_{Af}	Mole fraction of component A in the feed (–)
y_{Aj}	Mole fraction of component A in the bulk phase in bed i (–)
y_{Bf}	Mole fraction of component B in the feed (–)
y_{Bj}	Mole fraction of component B in the bulk phase in bed i (–)
$\langle y_{A2} \rangle$	Average mole fraction of the sorbate in the pores of the adsorbent pellet in bed 2 (–)
$y_{A,eq}$	Equilibrium mole fraction of component A for isomerization reaction (–)
y_{AL}	Mole fraction of component A at the exit of the column (–)

Greek Letters

ν_1	Dimensionless axial coordinate in the catalyst-bed region (–)
ν_2	Dimensionless axial coordinate in the adsorbent-bed region (–)

ω Fraction of the total length that is catalyst bed (–)
ζ_m Mass capacity factor (–)
θ_{ref} Coverage of adsorbent at y_{Af} and P_H (–)
τ Dimensionless time (–)

Subscripts

A n-Pentane
B Isopentane
I Hydrogen
T Total
f Feed
i Bed 1 (catalyst bed) or 2 (adsorbent bed)

Acknowledgments

The authors wish to acknowledge the support of King Fahd University of Petroleum & Minerals, Dhahran, Saudi Arabia during the course of this work.

References

Alpay, E., D. Chatsiriwech, L.S. Kershenbaum, C.P. Hull, and N.F. Kirkby, "Combined Reaction and Separation by Pressure Swing Adsorption," *Chem. Eng. Sci.*, **49**, 5845–5864 (1995).

Alpay, E., Y.S. Cheng, and L.S. Kershenbaum, "Simulation and Optimization of a Rapid Pressure Swing Reactor," *Comput. Chem. Eng.*, **22**, S45–S52 (1998).

Alpay, E., C.N. Kenney, and D.M. Scott, "Simulation of Rapid Pressure Swing Adsorption and Reaction Process," *Chem. Eng. Sci.*, **48**, 3173 (1993).

Breck, D.W., *Zeolite Molecular Sieves*, John Wiley & Sons, New York, 1974.

Bryant, P. and J. Spivey, "Hydroisomerization of n-C_5 and n-C_6 Mixtures on Zeolite Catalysts," *Ind. Eng. Chem. Process Des. Dev.*, **21**(4), 750–760 (1982).

Bryant, P. and A.J. Voorhies, "Hydroisomerization of n-Pentane Over a Zeolite Catalyst," *AIChE J.*, **14**(6), 852 (1968).

Chatsiriwech, D., E. Alpay, L.S. Kershenbaum, C.P. Hull, and N.F. Kirkby, "Enhancement of Catalytic Reaction by Pressure Swing Adsorption," *Catal. Today*, **20**, 351 (1994).

Fajula, F., D. McQueen, B.H. Chiche, A. Auroux, C. Guimon, F. Fitoussi, and P. Schulz, "A Multitechnique Characterization of the Acidity of Dealuminated Mazzite," *J. Catal.*, **161**, 587–596 (1996).

Fogler, H.S., *Elements of Chemical Reaction Engineering*, Prentice Hall, New York, 1992.

Gary, J., "Total Isomerization Process," U.S. Patent 4,709,117 (1987).

Glueckauf, E., "Formula for Diffusion into Spheres and their Application to Chromatography," *J. Chem. Soc.*, **51**, 1540 (1955).

Goto, S., T. Tagawa, and T. Omiya, "Dehydrogenation of Cyclohexane in a PSA Reactor Using Hydrogen Occlusion Alloy," *Chem. Eng Essays (Japan)*, **19**(6), 978 (1993).

Kadlec, R.H. and G.G. Vaporciyan, "Periodic Chemical Processing System," U.S. Patent 5,254,368 (1993).

Kirkby, N.F. and J.E. Morgan, "A Theoretical Investigation of Pressure Swing Reaction," *Trans. Inst. Chem. Eng.*, **72**, 541 (1994).

Lee, I.D. and R.H. Kadlec, "Effects of Adsorbent and Catalyst Distributions in Pressure Swing Reactors," *AIChE Symp. Ser.*, **84**, 167 (1989).

Lu, Z.P. and A.E. Rodrigues, "Pressure Swing Adsorption Reactors: Simulation of Three-Step One-Bed Process," *AIChE J.*, **40**, 1118 (1994).

Minkkinen, A., L. Mank, and S. Jullian, "Process for the Isomerization of C5/C6 Normal Paraffins with Recycling of Normal Paraffins," U.S. Patent 5,233,120 (1993).

Morbidelli, M., M. Mazzotti, R. Baciochi, and G. Storti, "Vapor-Phase SMB Adsorptive Separation of Linear/Nonlinear Paraffins," *Ind. Eng. Chem. Res.*, **35**, 2313 (1996).

Morbidelli, M., A. Servida, and G. Storti, "Simulation of Multicomponent Adsorption Bed. Model Analysis and Numerical Solution," *Ind. Eng. Chem. Fundam.*, **21**, 123 (1982).

Nitta, T., T. Shigetomi, and T. Katayama, "An Adsorption Isotherm of Multi-site Occupancy Model for Homogeneous Surface," *J. Chem. Eng. Jpn.*, **17**, 39–51 (1984).

Pines, H., K. Vetinskas, K. Assel, and I. Patieff, "Determination of Equilibrium Constants for Butanes and Pentanes," *J. Am. Chem. Soc.*, **67**, 631 (1945).

Runstraat, A., J. Grondelle, and R.A. Santen, "On the Temperature Dependence of the Arrhenius Activation Energy for Hydroisomerization Catalyzed by Pt/Mordenite," *J. Catal.*, **167**, 460–463 (1997a).

Runstraat, A., J. Grondelle, and R. Santen, "Microkinetics Modeling of the Hydroisomerization of n-Hexane," *Ind. Eng. Chem. Res.*, **36**, 3116–3125 (1997b).

Runstraat, A., J. Kamp, P. Stobbelaar, J. Grondelle, S. Krijnen, and R. Santen, "Kinetics of Hydroisomerization of n-Hexane over Platinum Containing Zeolites," *J. Catal.*, **171**, 77–84 (1997c).

Ruthven, D.M., M.M. Hassan, and N.S. Raghavan, "Numerical Simulation of a PSA System-Part I," *AIChE J.*, **31**(3), 385–392 (1985).

Ruthven, D.M. and N.S. Raghavan, "Numerical Simulation of a PSA System-Part III," *AIChE J.*, **31**(2), 1829 (1985).

Silva, J.A. and A.E. Rodrigues, "Sorption and Diffusion of n-Pentane in Pellets of 5A Zeolite," *Ind. Eng. Chem. Res.*, **36**, 493–500 (1997a).

Silva, J.A. and A.E. Rodrigues, "Fixed-Bed Adsorption of n-Pentane/Isopentane Mixtures in Pellets of 5A Zeolite," *Ind. Eng. Chem. Res.*, **36**, 3769–3777 (1997b).

Sircar, S., B.T. Carvill, J.R. Hufton, and M. Anand, "Sorption-Enhanced Reaction Process," *AIChE J.*, **42**(10), 2765–2772 (1996).

Skarstrom, C.W., "Method and Apparatus for Fractionating Gaseous Mixtures by Adsorption," U.S. Patent no. 2,944,627 (1960).

Vaporciyan, G.G. and R.H. Kadlec, "Equilibrium Limited Periodic Separating Reactors," *AIChE J.*, **33**, 1334 (1987).

Vaporciyan, G.G. and R.H. Kadlec, "Periodic Separating Reactors: Experiments and Theory," *AIChE J.*, **3**, 831 (1989).

Wakao, N. and S. Kaguei, *Heat and Mass Transfer in Packed Beds*, Gordon and Breach Science Publishers, New York, 1982.

Weisz, P.B., in *Advances in Catalysis and related Subjects*, D.D. Eley, P.W. Selwood, and P.B. Weisz (Eds.), Vol. 13, p. 157, Academic Press, London, 1962.